Methyl Viologen Anolyte Introducing Nitrate as Counter-Anion for an Aqueous Redox Flow Battery

Journal of The Electrochemical Society, 2021 **168** 100532
1945-7111/2021/168(10)/100532/8/$40.00 © 2021 The Electrochemical Society ("ECS"). Published on behalf of ECS by IOP Publishing Limited

Methyl Viologen Anolyte Introducing Nitrate as Counter-Anion for an Aqueous Redox Flow Battery

Sang-Soon Jang,[1,2] Se-Kook Park,[1] Sun-Hwa Yeon,[1] Kyoung-Hee Shin,[1] Haneul Song,[1] Han-Su Kim,[2] Yoon-Seok Jung,[3] and Chang-Soo Jin[1,z]

[1]*Korea Institute of Energy Research, Daejeon 305-343, Republic of Korea*
[2]*Department of Energy Engineering, Hanyang University, Seoul 04763, Republic of Korea*
[3]*Department of Chemical and Biomolecular Engineering, Yonsei University, Seoul 03722, Republic of Korea*

Among the redox active molecules, methyl viologen (MV) is the most promising redox species in an aqueous organic redox flow battery, featuring the stable redox reaction $MV^{2+}/MV^{\bullet+}$. Its electrochemical properties and solubility significantly depend on the counter-anion. Herein, we introduce the nitrate as a counter-anion to methyl viologen dication to obtain a new water-soluble methyl viologen compound (MVdN) and identify the effects of nitrate as counter-anion on electrochemical properties of methyl viologen. Nitrate leads to ~ 3.5 M solubility in water and good electrochemical reversibility ($i_{p,a}/i_{p,c} = 0.79$, $\Delta E = 54$ mV) with fast mass transfer ($D = 5.13 \times 10^{-5}$ $cm^2 \cdot s^{-1}$) of methyl viologen, which is superior to commonly used methyl viologen dichloride(MVdCl). Additionally, flow cell performance from 40 to 100 mA cm^{-2} exhibited 99% coulombic efficiency and comparable performance with MVdCl. Nitrate could be a promising choice as a counter anion to methyl viologen as aqueous redox active molecule.
 [DOI: 10.1149/1945-7111/ac2759]

Manuscript submitted October 20, 2020; revised manuscript received September 6, 2021. Published October 22, 2021.

Supplementary material for this article is available online

Redox flow battery (RFB) has attracted attention as one of the most promising technologies for the storage of renewable energy sources and peak-shifting.[1–3] RFB has many advantages including design flexibility, a long lifespan, and high energy efficiency.[4–6] RFB utilizes redox active materials dissolved in the electrolyte solution to store energy. The positive and negative electrolytes are stored in two separate reservoirs and pumped through the cell for energy conversion between electrical energy and chemical energy[1–3] The reservoir volume determines the capacity, and the size of the cell defines the power capability of the RFB.[7,8] Among various RFB systems, vanadium utilizing aqueous RFB (VRFB) is the most popular system and has been investigated on various approaches to performance.[9–13] Also, VRFB has been commercialized by numerous companies.[1,2] However, the corrosive electrolyte solution (e.g., concentrated sulfuric acid) and the high cost of vanadium limit its widespread application.[5,14,15]

Recently, organic redox molecules have emerged as a promising electroactive material and the new generation of RFBs for green energy storage to replace VRFB.[4,16–24] Various organic redox couples have so far been reported due to the merits of organic molecules, including the potentially low cost, tailorability and minimal environmental impact.[3,4,7,17–19,21,25,26] Among the many kinds of organic redox molecule candidates, viologen compounds have been widely used in electrochemical and electrochromic applications and feature the stable redox reaction V^{2+}/V^{+} as well as the tunability of the nitrogen substituents.[27–30] Up until now, many studies have reported using viologen compounds as redox active species in both aqueous and non-aqueous systems, such as the viologen/TEMPOL couple,[3] viologen polymer/TEMPO polymer couple,[21] MV/FcNCl,[31] $[(NPr)_2V]Cl_4$/N^{Me}-TEMPO[32] and MVTFSI/FcNTFSI,[33] etc.

Because the characteristic ionic states of viologen salts structurally consist of viologen dication and counter-anions, its color, electrochemical properties and solubility are controlled by the substituents and the counter-anions.[27,28] Substituents of viologen affect both the solubility and reversible potential. For instance, in the aqueous system, methyl viologen, the form with the shortest alkyl substituent, has a higher solubility (3.0 M) because increased size of organic substituents on the nitrogen atoms lowers the hydrophilicity of the corresponding viologen compounds.[4] Counter anions, as well as substituents, have an influence on the electrochemical properties, color and solubility of viologen compounds. There are two types of counter anion for viologen in terms of solubility: one is relatively large counter-anions (NO_3^-, ClO_4^-, BF_4^- or PF_6^-), and the other is hard bases in the Lewis sense (F^-, Cl^-, Br^- or I^-). The effects of the anions on the solubility of viologen vary with solution condition (in organic solution or aqueous solution) and charge state (viologen dication or radical-cation). The only common anion to impart solubility to radical-cation salts in both aqueous and non-aqueous solutions is nitrate.[27,28] In an aqueous solution, halide ions were widely researched as a counter anion for viologen dication.[34–36] However, bromide and iodide give very lower solubility to viologen compounds and cause precipitate of viologen radical.[27–29] Chloride, which imparts a good solubility to both radical and dication, was commonly used as counter-anion in aqueous systems. For those reasons, methyl viologen dichloride (MVdCl) has been mainly used as a redox active molecule in aqueous redox flow batteries. Although MVdCl has high solubility (~3 M) and rapid electrochemical kinetics (diffusion coefficient and electron transfer rate constant), solubility and electrochemical kinetics of methyl viologen could be further improved without precipitation by introducing appropriate counter-anions, expecting improved performance in RFB.

Herein, we introduce nitrate as a counter anion to the methyl viologen dication (MVdN) to obtain a new water-soluble methyl viologen compound, expecting that nitrate imparts high solubility to methyl viologen dication. And then we also compare the effects of nitrate and chloride as counter-anions on electrochemical properties of methyl viologen as redox active molecule for aqueous redox flow battery. MVdN was synthesized by a two-step process (Scheme 1). The electrochemical properties were investigated using cyclic voltammetry (CV) and rotating disk electrode (RDE). Then, the identified electrochemical properties of MVdN were compared with MVdCl. MVdN exhibited very high solubility in water (~3.5 M), which is higher than that of MVdCl the commonly used methyl viologen form as redox active molecule. Also, MVdN has good electrochemical reversibility ($i_{p,a}/i_{p,c} = 0.79, \Delta E = 54$ mV) with fast mass transfer ($D = 5.13 \times 10^{-5}$ $cm^2 \cdot s^{-1}$). 1 M MVdN/TEMPOL flow cell tests in $NaNO_3$ aqueous solution exhibited high coulombic efficiency of over 95% at 40 mA·cm^{-2} and comparable performance with MVdCl.

Experimental

Materials and instrumentation.—4-Hydroxyl-2,2,6,6-tetramethylpiperidine (TEMPOL, TCI, >98.0%), Methyl viologen dichloride

[z]E-mail: csjin@kier.re.kr

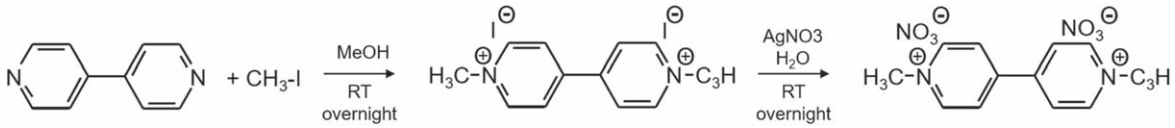

Scheme 1. Schematic representation of the synthesis of the methyl viologen dinitrate ($MV^{2+}*2NO_3^-$) by two-step process.

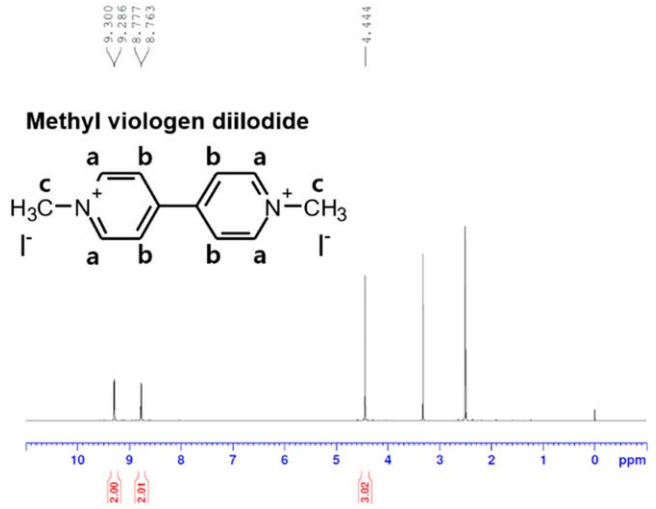

Figure 1. ^{1}H NMR (DMSO-d_6, 500 MHz, ppm) of MVdI.

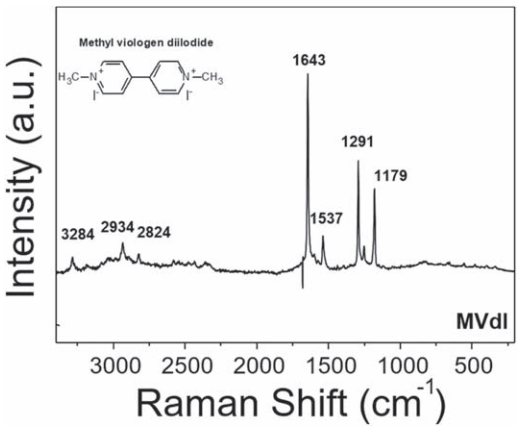

Figure 2. Raman spectra of MVdI.

(Sigma-Aldrich), 4,4′-bipyridinium (Chem-Tree, 98%), sodium nitrate (Sigma-Aldrich, ⩾99%), sodium chloride (JUNSEI, 99.5%), silver nitrate (Sigma-Aldrich, ⩾99%), methanol (Sigma-Aldrich, 99.9%), and acetonitrile (Ducksan) were used as received without any further purification. ^{1}H NMR (nuclear magnetic resonance) spectra were recorded using a Bruker Avance 500 MHz spectrometer in deuterated dimethylsulfoxide (DMSO-d_6) at 298 K. Chemical shifts are reported in parts per million (ppm, δ scale) relative to tetramethylsilane. Raman spectra were recorded in the range from 200 to 3400 cm^{-1} on a DXD Raman microscope (Thermo Fisher Scientific) with nanometer laser excitation. Elemental analysis (C, H, N and O) was performed using a Thermo Scientific Flash 200 elemental analyzer.

Synthesis of 1,1′-dimethyl-4,4′-bipyridinium diiodide (MVdI).—4,4′-Bipyridyl (46.86 g, 0.3 mol) was dissolved in methanol (500 ml), and then, methyl iodide (74.71 ml) was slowly added, followed by stirring at room temperature overnight. After the solvent was evaporated by a rotary evaporator at 40 °C under vacuum, the precipitate was filtered off, washed with methanol and dried (60 °C, vacuum). The methyl viologen iodide was obtained as a powder (128.14 g, 97.05%, 0.29 mol). ^{1}H NMR (500 MHz, DMSO-d_6, 25 °C): δ (ppm) = 9.30 (d, J = 6.6 Hz, 4H), 8.76 (d, J = 6.5 Hz, 4H), 4.44 (s, 3H)(Fig. 1); Raman 3108, 3045, 2963, 1647, 1538, 1292, 1187, 1043 cm^{-1} (Fig. 2). Elemental analysis calcd (%) for $C_{12}H_{14}N_2I_2$: C 32.75, H 3.21, N 6.37; found: C 32.58, H 3.15, N 3.63.

Synthesis of 1,1′-dimethyl-4,4′-bipyridinium dinitrate (MVdN).—Ion exchange from iodide to nitrate was conducted by dissolving methyl viologen iodide (128.12 g, 0.29 mol) in deionized water. Afterward, silver nitrate (110.40 g, 0.65 mol) was carefully added, followed by stirring at room temperature overnight. The precipitate was removed by filtration and then washed with deionized water (each two times). After the filtered solution was recrystallized at 60 °C, the crude product was washed with acetonitrile two times to obtain pure methyl viologen dinitrate. After drying at 60 °C, the pure methyl viologen dinitrate was obtained as a powder (73.34 g, 80.02%, 0.24 mol). ^{1}H NMR (500 MHz, DMSO-d_6, 25 °C): δ (ppm) = 9.30 (d, J = 6.6 Hz, 4H), 8.78 (d, J = 6.6 Hz, 4H), 4.43 (s, 3H)(Fig. 3); Raman 3284, 2934, 2824, 1634, 1537, 1291, 1179 cm^{-1} (Fig. 4). Elemental analysis calcd (%) for $C_{12}H_{14}N_4O$: C 46.45, H 4.55, N 18.06, O 30.94; found: C 46.32, H 4.50, N 19.22, O 28.33.

Cyclic voltammetry.—Cyclic voltammetry (CV) experiments were conducted using a CHI 760 model (CH Instruments, Inc.) and performed using a three-electrode cell consisting of an Ag/AgCl aqueous reference electrode (Thermo Fisher, Orion™ 900200 Sure-Flow™), platinum wire electrode (ALS Co., Ltd., 0.5 mm diameter) and glassy carbon working electrode (BAS Inc., 3.0 mm diameter). The glassy carbon working electrode was polished with 0.05 μm alumina (ALS Co., Ltd.) and washed with deionized water before each new set of measurements. Twenty-one segments of CV were recorded at various scan rates (1000, 500, 200, 100, 50, 20 mV s^{-1}) in 1 M $NaNO_3$ and NaCl aqueous electrolytes. The half-wave potential $E_{1/2}$ (the average of the cathodic and anodic peak potentials) and the reduction and oxidation peak current ($I_{p,c}$) were calculated using the CH-760d baseline computer program.

Rotating disk electrode.—Rotating disk electrode (RDE) experiments were conducted using an RRDE-3A (ALS Co., Ltd.) performed using a three-electrode cell consisting of an RRDE GC Ring/GC Disk electrode (BAS Inc., 4.0 mm disk diameter) as the working electrode, and the counter electrode and reference electrode were the same as used in the CV experiments. The RRDE GC Ring/GC Disk electrode was polished with 0.05 μm alumina (ALS Co., Ltd.) and washed with deionized water before each new set of measurements. Before CV and RDE measurements, the electrolytes were deoxygenated for 1 h. During measurements, argon purging was conducted to provide a blanket of argon gas over the solution surface.

Linear sweep voltammetry (LSV) was conducted using a CHI 760 model in a three-electrode configuration. An RRDE GC Ring/GC Disk electrode (BAS Inc., 4.0 mm disk diameter) was used as the working electrode. The counter electrode and reference electrode were the same as used in the CV experiments. Before each new set of measurements, the RRDE GC Ring/GC Disk electrode was polished with 0.05 μm alumina (ALS Co., Ltd.) and washed with

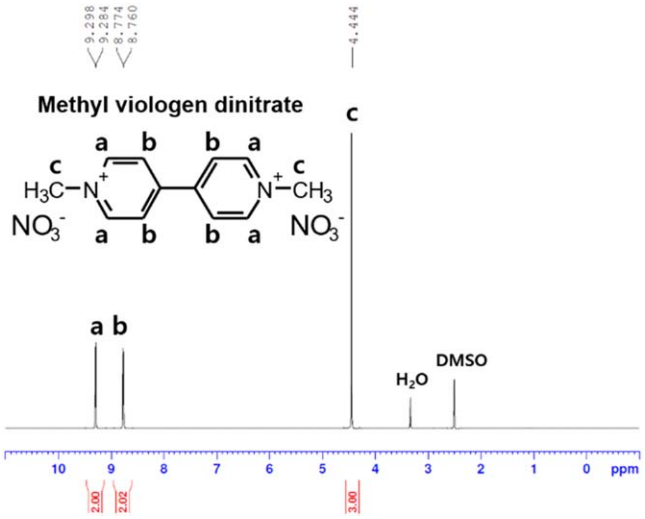

Figure 3. ^{1}H NMR (DMSO-d_6, 500 MHz, ppm) of MVdN.

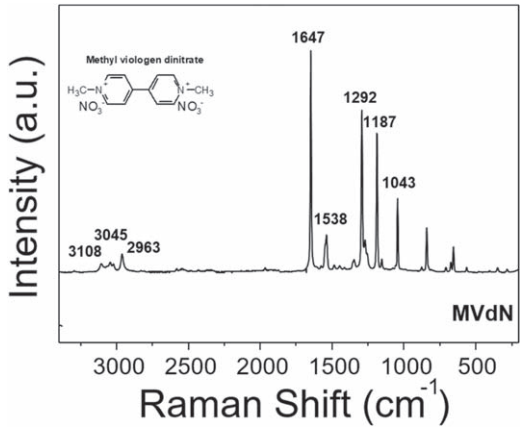

Figure 4. Raman spectra of MVdN.

deionized water. The electrode was then rotated manually at 600 to 3000 rpm with a 300 rpm increment. LSV scans were recorded at a rate of 5 mV s^{-1}. The liming currents were measured at −0.9 V vs Ag/AgCl and plotted vs the square root of the rotation rate (ω). This Levich plot (limiting currents vs the square root of the rotation rate) yields the corresponding diffusion coefficient D using the Levich equation:[37]

$$i = 0.62nFAD^{2/3}C\omega^{1/2}\nu^{-1/6} \quad [1]$$

where i is the limiting current, n is the number of electrons per redox reaction (n=1), F is the Faraday constant (96485 C mol^{-1}), A is the surface area of the electrode (0.1257 cm^2), D is the diffusion coefficient ($cm^2 \cdot s^{-1}$), C is the active species concentration (5.0×10^{-3} M), ω is the rotation rotating angular velocity (rad s^{-1}), and ν is the kinematic viscosity (0.01 $cm^2 \cdot s^{-1}$).

The inverse current measured potential at each was plotted vs the square root of the rotation rate. The Koutecký-Levich equation was used to fit the lines of the Koutecký-Levich plot (inverse current vs the square root of the rotation rate).[37]

$$\frac{1}{\mathrm{i}} = \frac{1}{i_k} + \frac{1}{0.620}nFAcD^{2/3}\nu^{-1/6}\omega^{1/2} \quad [2]$$

where i_k is the mass-transfer-independent kinetic current. Subsequently, i_k was plotted vs the overpotential (η). The vertical-axis intercept of the Tafel plot (log($|i_K|$) vs overpotential) allows the determination of i_0 (log[$i_k(0)$] = log($|i_0|$)) using the Tafel equation:[37]

$$\log_{10}(i) = \log_{10} i_0 + \frac{\alpha nF\eta}{RT} \quad [3]$$

where i_0 is the exchange current in amp, α is the transfer coefficient, R is the universal gas constant (8.314 J K^{-1} mol^{-1}), and T is the temperature (298 K). Through the slope of the Tafel plot, the transfer coefficient α was calculated, and the electron transfer rate constant k_0 was calculated using the following equation:[37]

$$k_0 = \frac{i_0}{nFcA} \quad [4]$$

Flow cell test.—The flow cells for the MVdN/TEMPOL couple were tested using Maccor series 4000 Battery Test System (Maccor Inc.) at 298 K in voltage range of 1.6–0.5 V at current densities ranging from 40 to 100 mA·cm^{-2}. The flow cell was assembled with two glass end plates, two graphite bipolar plates, two copper current collectors, two graphite felts (4 mm thickness, XF-30A, Toyobo Co., Ltd.) and an anion exchange membrane (AMV, 120 um thickness, Selemion, Japan). The active area of the electrode and the separator was 30 cm^2. Under the 1:1 volume ratio of catholyte and anolyte, 20 ml for each of the catholyte and anolyte was circulated at a flow rate of 40 ml·min^{-1} through the electrodes using Masterflex L/S peristaltic pump (Cole-Parmer, Vernon Hills, IL). The electrolytes contain $NaNO_3$ 1.5 or 2 M as supporting electrolytes and 0.5 or 1 M active materials. Both electrolytes were purged with argon at 30 min before cell cycling. AMV was used after immerging in a supporting electrolyte at room temperature overnight. Before the cell test, supporting electrolyte was circulated through the cell for swelling the felt and AMV.

Results and Discussion

Electrochemical properties.—The electrochemical properties of MVdN were studied by cyclic voltammetry (CV). Figure 5 shows the CV curves of MVdCl and MVdN in the 1 M sodium chloride or sodium nitrate electrolyte at different scan rates. The overall CV exhibited the scan rate dependence, indicating that it is a diffusion-controlled process. As shown in Fig. 5d, the positions of the half-wave potentials ($E_{1/2}$) of both MVdCl and MVdN remain almost constant with the scan rate. The $E_{1/2}$ of the $MV^{2+}/MV^{\bullet+}$ redox couple complexed with chloride and nitrate counter anions were –0.655 V and −0.652 vs Ag/AgCl, respectively (Table II). The potential difference was only −0.003 V, and these values were almost identical. The counter anion can have an influence on the electrode potential with regards to the absorption and solution-phase association.[27] Particularly, in the case of heptyl viologen, it has been reported that the absolute value of the $E_{1/2}$ of the first reduction step follows the inverse order of the counter anion radius.[38] Likewise, for methyl viologen, this difference may be attributed to anion radius order (Cl^-: 0.18 nm, NO_3^-: 0.33 nm).[39,40] The $E_{1/2}$ of MVdN was still sufficiently high, which represents the highest value so far for an organic RFB.[4,41–45]

Using the cyclic voltammetry method, the coulombic reversibility of a redox species can be determined by comparing the anodic and cathodic peak currents from the resulting voltammograms at several scan rates.[46,47] As known, for a Nernstian, the peak current ratio is nearly equal to unity regardless of the scan rate.[37] As seen in Table I, the peak current ratio of MVdN (0.79) was closer to unity than that of MVdCl (0.73), indicating that the MVdN redox reaction was more reversible than that of MVdCl. Additionally, there was the tendency that the peak current increase with an increasing scan rate was higher in MVdN (Fig. 5c). At the same scan rate, the much higher peak current in static solutions may be attributed to the fast mass transfer of MVdN. The CV studies exhibit the sufficiently low redox potential, fast mass transfer and remarkable coulombic

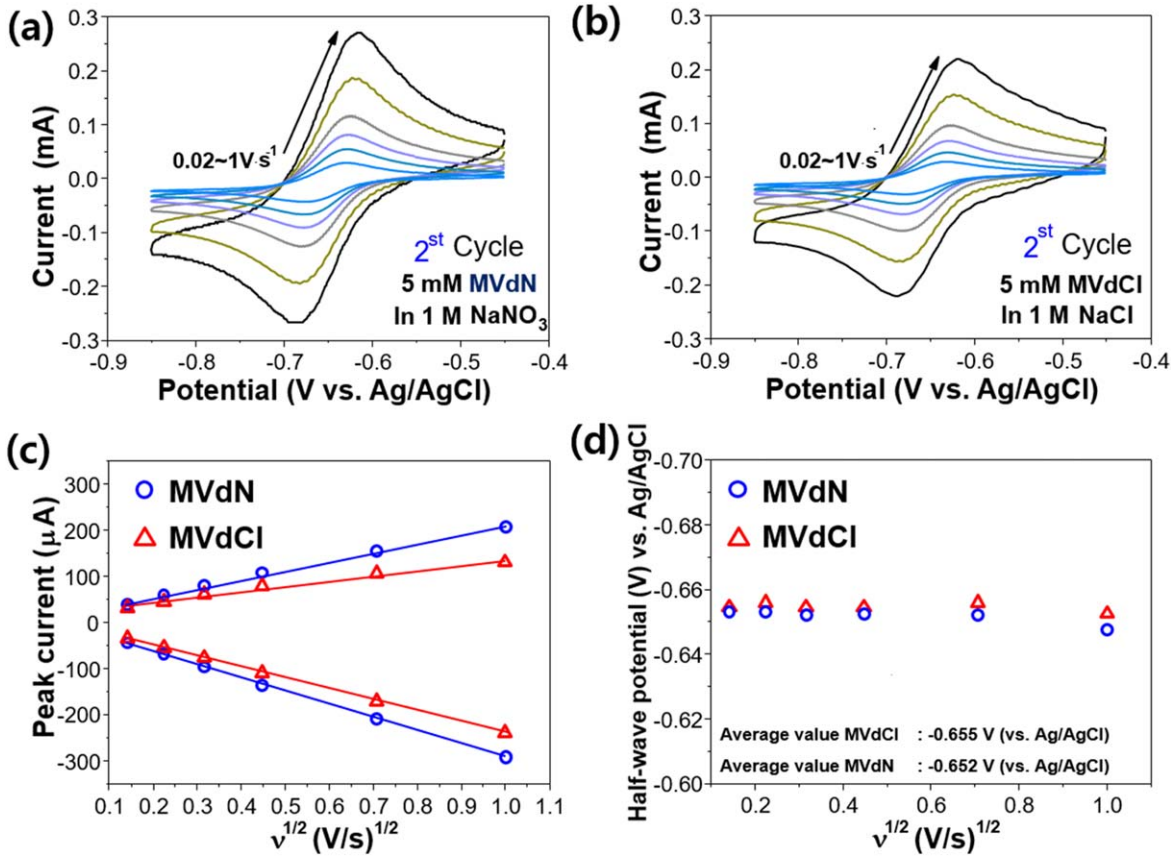

Figure 5. Cyclic voltammograms of (a) 5 mM MVdN in 1 M $NaNO_3$, (b) 5 mM MVdCl in 1 M NaCl electrolyte, (c) Linear relationship between peak currents vs the square root of scan rates, (d) Half-wave potentials of constant positions with respect to the square root of scan rates.

Table I. Peak current and its ratios of MVdN and MVdCl with respect to the square root of scan rates, respectively.

	MVdN			MVdCl		
$\nu^{1/2}$ $(V/s)^{1/2}$	$I_{p,c}$	$I_{p,a}$	$I_{p,c}/I_{p,a}$ (mA)	$I_{p,c}$	$I_{p,a}$	$I_{p,c}/I_{p,a}$
1	0.207	0.293	0.706	0.130	0.241	0.539
0.707	0.154	0.209	0.737	0.107	0.172	0.620
0.447	0.108	0.136	0.794	0.080	0.19	0.729
0.316	0.080	0.097	0.827	0.061	0.077	0.783
0.224	0.058	0.069	0.849	0.045	0.055	0.823
0.141	0.038	0.045	0.846	0.030	0.035	0.864

reversibility of MVdN, implying the high diffusion coefficient and electron transfer rate constant.

To further investigate the electrochemical properties, we measured the electron transfer rate constant and diffusion coefficient of MVdN and MVdCl in the aqueous electrolyte by using a rotating disk electrode (RDE). To obtain the electron transfer rate constant and diffusion coefficient in aqueous electrolyte, RDE was conducted at 10 $mV{\cdot}s^{-1}$ and different rotating rates from 600 to 3000 rpm (in Fig. 6). Figure 6c displays the limiting current at the square root of different rotation rates for both MVdN and MVdCl, showing the linear correlation. This linear correlation of the Levich plot indicates that both MVdN and MVdCl follow a mass-transport controlled process. From the slope of the Levich plot (Fig. 5c), diffusion coefficients of MVdN and MVdCl were calculated to be 5.13×10^{-5} and 1.95×10^{-5} $cm^2{\cdot}s^{-1}$ using the Levich equation (Eq. 1).

The calculated diffusion coefficient of MVdN was more than two times higher compared to that of MVdCl, which is remarkable when compared with other organic redox molecules.[3,4,7,17,18,21,26] This result showed a similar tendency with the peak current ratio of the CV result. These tendencies suggest the very fast mass transfer of methyl viologen when nitrate was used as the counter anion. Since the electrode reactions are controlled by diffusion, a fast diffusion process of MVdN is expected to produce low activation polarization loss, which is favored for the power performance of the flow battery.[48,49]

Generally, the diffusion coefficient dominantly depends on the ionic radius. Additionally, MVdN (310.3 g) is heavier than MVdCl (257.2 g). However, in the aqueous solution, MVdN has a higher diffusion coefficient than MVdCl, implying that the counter anion affects the diffusion process of methyl viologen. In an aqueous solution, viologen species associate between the viologen dication and anions and the extent of association may affect the electrochemical properties of the viologen dication.[27,50–52] The more highly associated viologen dication will diffuse more slowly through the solution. In other words, a smaller diffusion coefficient in water implies that the ion association is more extensive due to the rather low values, suggesting that methyl viologen may weakly associate with nitrate rather than chloride. The higher diffusion coefficient of MVdN may be explained by the weak association between methyl viologen and nitrate.

Koutecký-Levich plots (Figs. 6d, 6e), which show the linear relationship between the reciprocal of the corresponding current and the square root of the rotation rates at selected overpotentials, provide the mass-transfer independent current i_k (Eq. 2). The i_k values were used to obtain the Tafel plot (Fig. 6f), which in turn was used to calculate the electron transfer rate constants for the reduction of MVdN and MVdCl. From Eq. 4, the electron transfer rate constants of MVdN and MVdCl were obtained to be 9.68×10^{-3}

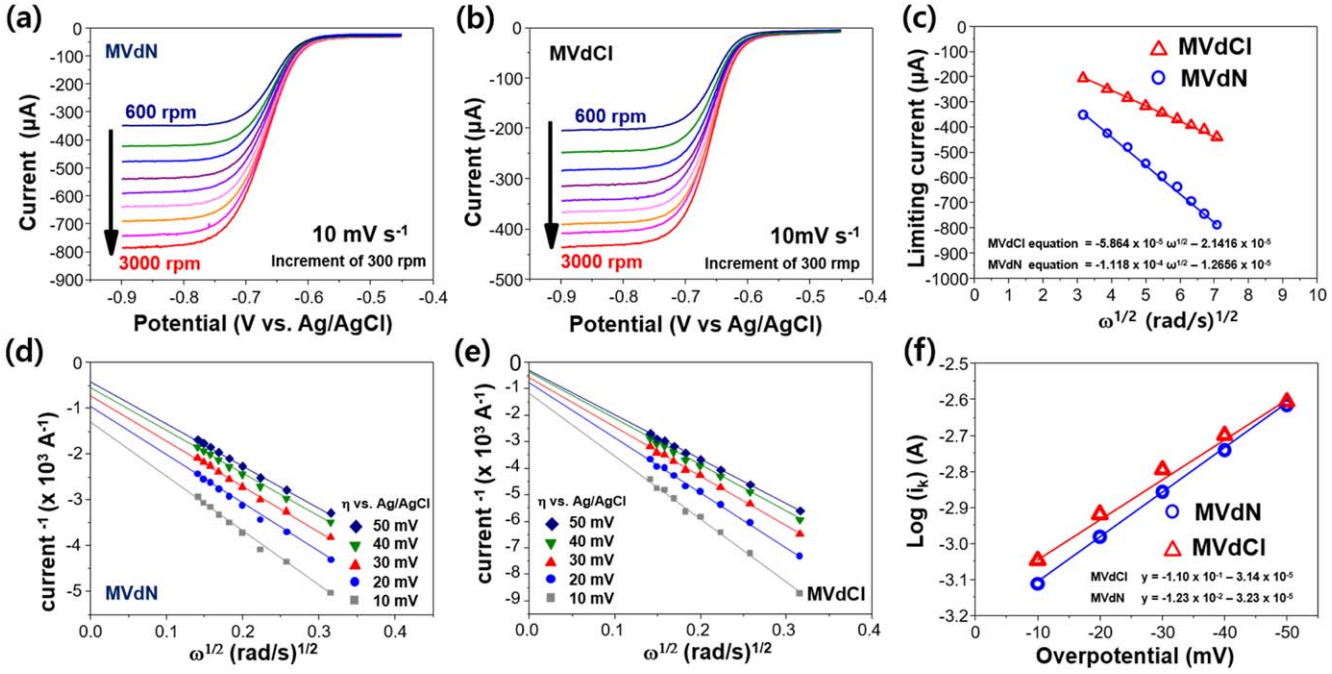

Figure 6. Rotating disk electrode (RDE) experiments of 5 mM MVdN in 1 M $NaNO_3$ or MVdCl in 1 M NaCl aqueous electrolyte. (a), (b) Linear sweep voltammograms varying rotation rates from 600 to 3000 rpm of MVdN and MVdCl, respectively. (c) Levich plot of limiting current at 0.9 V (vs Ag/AgCl) vs the square root of rotation rates. (d), (e) Koutecký-Levich plot of inverse current vs inverse square root of rotation rates for MVdN and MVdCl, respectively. (f) Tafel plot of log i_k vs overpotential from 10 mV to 50 mV for MVdN and MVdCl, respectively.

Table II. Electrochemical data of MVdN and MVdCl in 1 M $NaNO_3$ or NaCl aqueous solution. ($E_{1/2}$, δE_p, I_{pc}/I_{pa} are average values for different scan rates).

Viologen compound	$E_{1/2}$ V vs Ag/Ag^+	ΔE_p mV	$I_{p,c}/I_{p,a}$	D (10^{-5} $cm^2 \cdot s^{-1}$)	k_0 (10^{-2} $cm \cdot s^{-1}$)
MVdN	−0.652	53.7	0.793	5.13	0.968
MVdCl	−0.655	56.3	0.726	1.95	1.19

and 1.19×10^{-2} $cm \cdot s^{-1}$. The calculated electron transfer rate constant of MVdCl was slightly higher than that of MVdN, and both values were comparable to that of reported organic redox molecules.[3,4,7,17,18,21,26] The higher electron transfer rate constant of MVdCl may be attributed to the catalytic effect of Cl^- dissolved in the electrolyte that is preferentially absorbed in the electrical double layer.[53,54] The absorbed Cl^- perturbs the solvation sphere of the molecules and incorporates into the first coordination shell, forming a chloride-bridge inner sphere path. This path provides a fast rate for the redox reaction because Cl^- complex can approach the electrode to shorter distances than the other complexes hence enhances the overlap of the molecules with an electrode and thereby catalyze electron transfer.[27,55] All of these presented results suggest that faster mass transfer and better coulombic reversibility of methyl viologen were obtained by employing nitrate as a counter anion. In addition, these improved electrochemical properties can also benefit cell performance at high current densities.

Flow cell performance.—Flow cell performance tests of MVdN coupled with TEMPOL were conducted at room temperature at a concentration of 0.5 M for both catholyte and anolyte in 1.5 M $NaNO_3$ aqueous solution and 1 M for both in 2 M $NaNO_3$ additionally. TEMPOL, which is inexpensive cathode material and has a high solubility in water was used as a catholyte.[21,56] By employing $NaNO_3$ as a supporting electrolyte, NO_3^- anion can play the role of both counter anion and charge carrier during charge-discharge cycling. The rate performance was conducted using 0.5 M concentration from 40 to 100 mA·cm^{-2} with a 10 mA cm^{-2} increment, giving theoretical capacity as 13.4 Ah L^{-1}. As seen in Fig. 7a, the discharge capacity output was delivered 9.97Ah·l^{-1} at 40 mA·cm^{-2} to 3.39 Ah·l^{-1} at 100 mA·cm^{-2}. Up to 60 mA·cm^{-2}, no significant decreased capacity output (72% theoretical capacity delivery) was observed with an energy efficiency of over 61%. Overall decreased capacity output was due to the increased overpotential with increased current density. Coulombic efficiency remained over 99% for every current density, showing the dependence of energy efficiency on voltage efficiency. Although capacity decay was observed at 100 mA·cm^{-2} due to tight increment (10 mA·cm^{-2}) with the 4th cycle at each increment, excellent efficiencies were demonstrated, which corresponded to good electrochemical properties of MVdN. A continuous cycling test was conducted at 40 mA·cm^{-2} showing an average high coulombic efficiency of 99% and capacity retention of 70% and charge-discharge voltage plateau at 1.34 and 1 V over 100 cycles. The observed capacity decay (0.89% per hour or 21.4% per day) is mainly due to the side reaction of TEMPOL. It is well known that $TEMPO^+$ reacts with OH^- so that made the catholyte acidic, causing the loss of TEMPOL (Fig. S1 available online at stacks.iop.org/JES/168/100532/mmedia) and its tendency is accelerated by high concentrations.[57,58] And the results of comparison tests with MVdN and MVdN conducted at 30 mA·cm^{-2} and 1:2 volume ratio of anolyte (15 ml) and catholyte (30 ml) exhibited that MVdN is much superior in capacity retention (Fig. S2).

The higher concentration of MVdN/TEMPOL cell test was performed with 1 M for both catholyte and anolyte in a 2 M $NaNO_3$ solution. The cell then cycled at a constant current of 40 mA·cm^{-2}.

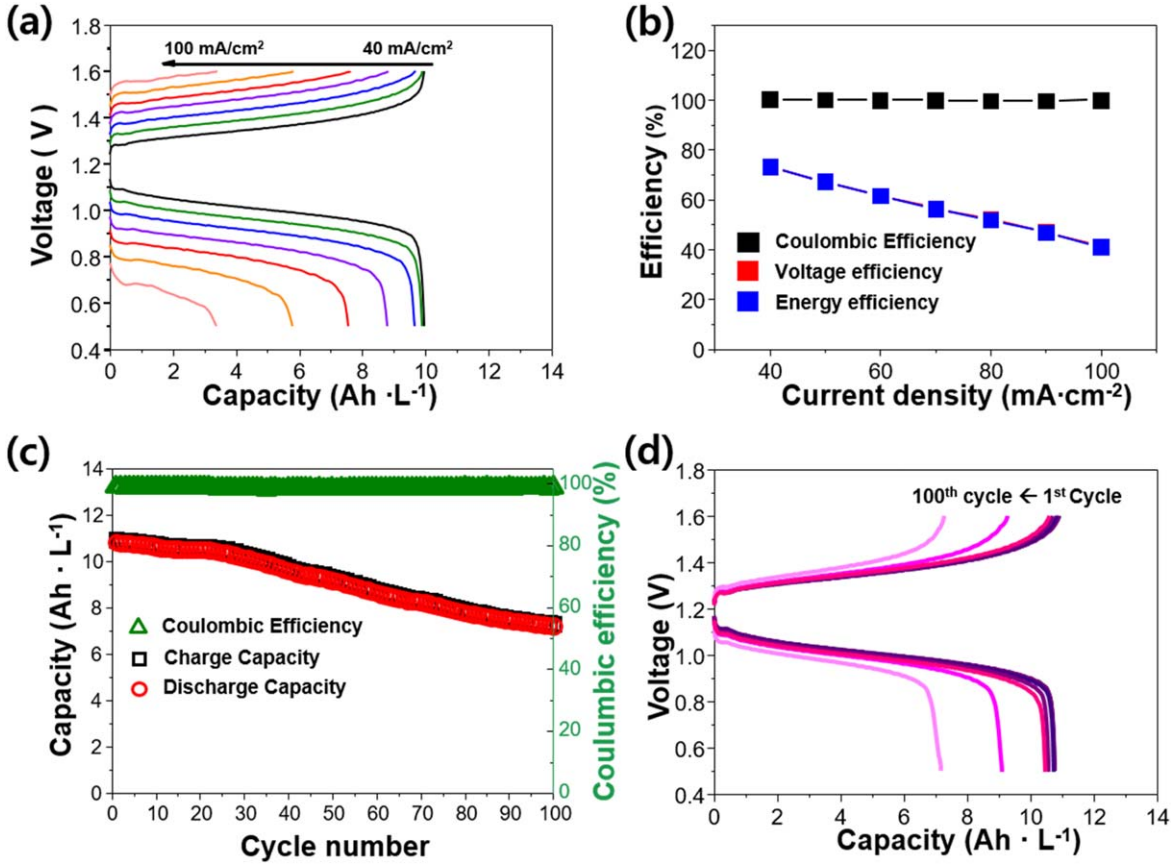

Figure 7. (a) Plots of charge and discharge profiles of TEMPOL/MVdN (0.5 M) at the cycling rates from 40 to 100 mA·cm^{-2} with increments of 10 mA·cm^{-2}. (b) Plots of coulombic, voltage and energy efficiency vs current density. (c) Capacity vs cycle number at current density 40 mA·cm^{-2} over continuous flow cell test. (d) Cell voltage vs capacity at 1, 2, 5, 10, 20, 50 and 100th cycles for representative capacity retention profile.

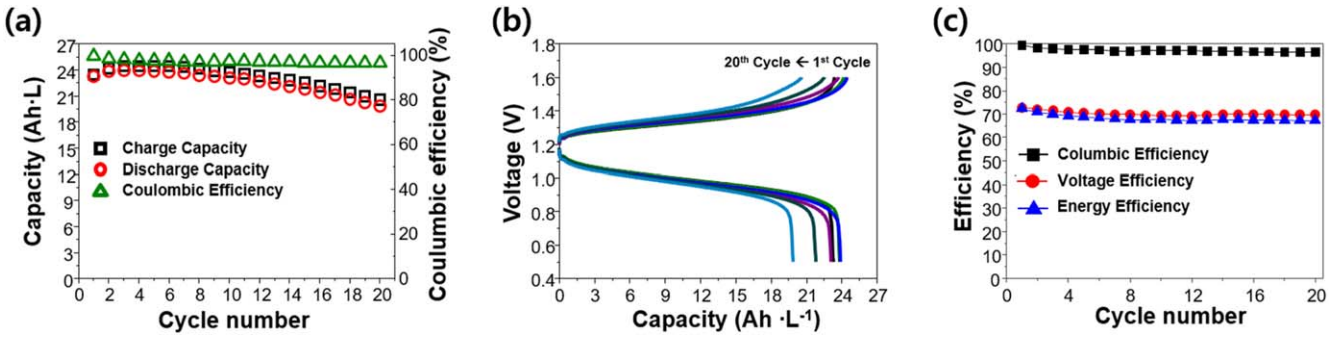

Figure 8. (a) Plots of capacity and coulombic efficiency vs cycle number of TEMPOL/MVdN (1 M) at current density 40 mA·cm^{-2}. (b)) Cell voltage vs capacity at 1, 2, 5, 10, 15 and 20th cycles for a representative capacity retention profile. (c) Plots of coulombic, voltage and energy efficiency vs cycle number.

The initial coulombic efficiency, voltage efficiency and energy efficiency of the RFBs were 99.4%, 72.8% and 72.4%, respectively (Fig. 8c). The coulombic efficiency remained over 95% and capacity retention was over 69% during cycles. The measured capacity and energy densities were 23.3 Ah·l^{-1} and 11.4 Wh·l^{-1}, corresponding the 87% and 68% of the theoretical value, respectively (cell voltage = 1.26 V). As seen in Fig. 8, the results were presented only until the 20th cycle. It may seem that the side reaction of TEMPOL was accelerated after 10 cycles. By utilizing improved electrochemical properties and reversibility of methyl viologen as an anolyte, it is expected that enhanced power performance was demonstrated. As a result, comparable flow cell performance was observed. Further investigation to identify the power performance and improve overall flow cell performance using MVdN will be needed, together with the researches for stable and inexpensive catholyte.

Conclusions

In conclusion, we introduced nitrate as a counter-anion to methyl viologen the aqueous redox active molecule. The nitrate leads to high solubility (~3.5 M) of methyl viologen and good electrochemical properties, which is superior to commonly used methyl viologen dichloride. Notably, the diffusion coefficient (D = 5.13 × 10^{-5} cm^2·s^{-1}) was more than two times higher than that of MVdCl the commonly used form of methyl viologen, which was attributed to the weak ion association of methyl viologen with nitrate. MVdN/

TEMPO flow cell tests demonstrated excellent coulombic efficiency (99%). The nitrate, giving an expectation of the fast and reversible charge-discharge performance of methyl viologen, represents a promising choice as counter-anion to methyl viologen for aqueous redox active molecule.

Acknowledgments

This research was supported by a grant from the R&D Program (2018M1A2A2063356 and 2019M3D1A2104106) funded by NRF, R&D Program (20007882 and 20007034) funded by the Ministry of Trade, Industry and Energy, R&D Program (P0009795) funded by the KIAT, and R&D Program (C0-5501-1 and C1-2408) funded by the KIER of Republic of Korea, respectively. No potential conflict of interest was reported by the authors.

ORCID

Sang-Soon Jang https://orcid.org/0000-0003-2908-6867
Yoon-Seok Jung https://orcid.org/0000-0003-0357-9508

References

1. W. Wang, Q. Luo, B. Li, X. Wei, L. Li, and Z. Yang, "Recent progress in redox flow battery research and development." *Adv. Funct. Mater.*, **23**, 970 (2013).
2. Z. Yang, J. Zhang, M. C. Kintner-Meyer, X. Lu, D. Choi, J. P. Lemmon, and J. Liu, "Electrochemical energy storage for green grid." *Chem. Rev.*, **111**, 3577 (2011).
3. B. Dunn, H. Kamath, and J.-M. Tarascon, "Electrical energy storage for the grid: a battery of choices." *Science*, **334**, 928 (2011).
4. T. Liu, X. Wei, Z. Nie, V. Sprenkle, and W. Wang, "A total organic aqueous redox flow battery employing a low cost and sustainable methyl viologen anolyte and 4-HO-TEMPO catholyte." *Adv. Energy Mater.*, **6**, 1501449 (2016).
5. P. Alotto, M. Guarnieri, and F. Moro, "Redox flow batteries for the storage of renewable energy: A review." *Renew. Sustain. Energy Rev.*, **29**, 325 (2014).
6. M. Skyllas-Kazacos, M. Chakrabarti, S. Hajimolana, F. Mjalli, and M. Saleem, "Progress in flow battery research and development." *J. Electrochem. Soc.*, **158**, R55 (2011).
7. T. Janoschka, N. Martin, M. D. Hager, and U. S. Schubert, "An aqueous redox-flow battery with high capacity and power: the TEMPTMA/MV system." *Angew. Chem. Int. Ed.*, **55**, 14427 (2016).
8. Y. Yao, J. Lei, Y. Shi, F. Ai, and Y.-C. Lu, "Assessment methods and performance metrics for redox flow batteries." *Nat. Energy*, **6**, 582 (2021).
9. S.-H. Yeon, J. Y. So, J. H. Yun, S.-K. Park, K.-H. Shin, C.-S. Jin, and Y. J. Lee, "Effect of phosphate additive for thermal stability in a vanadium redox flow battery." *Journal of Electrochemical Energy Conversion and Storage*, **14**, 4 (2017).
10. C.-S. Jin, J.-Y. So, K.-H. Shin, E.-B. Ha, M. J. Choi, S.-K. Park, Y.-J. Lee, and S.-H. Yeon, "Effect of organophosphorus compound additives for thermal stability on the positive electrolyte of a vanadium redox flow battery." *J. Appl. Electrochem.*, **48**, 1019 (2018).
11. K.-H. Shin, C.-S. Jin, J.-Y. So, S.-K. Park, D.-H. Kim, and S.-H. Yeon, "Real-time monitoring of the state of charge (SOC) in vanadium redox-flow batteries using UV–Vis spectroscopy in operando mode." *Journal of Energy Storage*, **27**, 101066 (2020).
12. S. Roe, C. Menictas, and M. Skyllas-Kazacos, "A high energy density vanadium redox flow battery with 3 M vanadium electrolyte." *J. Electrochem. Soc.*, **163**, A5023 (2015).
13. M. Skyllas-Kazacos and F. Grossmith, "Efficient vanadium redox flow cell." *J. Electrochem. Soc.*, **134**, 2950 (1987).
14. A. Z. Weber, M. M. Mench, J. P. Meyers, P. N. Ross, J. T. Gostick, and Q. Liu, "Redox flow batteries: a review." *J. Appl. Electrochem.*, **41**, 1137 (2011).
15. W. Wang, Z. Nie, B. Chen, F. Chen, Q. Luo, X. Wei, G. G. Xia, M. Skyllas-Kazacos, L. Li, and Z. Yang, "A new Fe/V redox flow battery using a sulfuric/chloric mixed-acid supporting electrolyte." *Adv. Energy Mater.*, **2**, 487 (2012).
16. Y. Xu, Y.-H. Wen, J. Cheng, G.-P. Cao, and Y.-S. Yang, "A study of tiron in aqueous solutions for redox flow battery application." *Electrochim. Acta*, **55**, 715 (2010).
17. B. Huskinson, M. P. Marshak, C. Suh, S. Er, M. R. Gerhardt, C. J. Galvin, X. Chen, A. Aspuru-Guzik, R. G. Gordon, and M. J. Aziz, "A metal-free organic–inorganic aqueous flow battery." *Nature*, **505**, 195 (2014).
18. B. Yang, L. Hoober-Burkhardt, F. Wang, G. S. Prakash, and S. Narayanan, "An inexpensive aqueous flow battery for large-scale electrical energy storage based on water-soluble organic redox couples." *J. Electrochem. Soc.*, **161**, A1371 (2014).
19. T. B. Schon, B. T. McAllister, P.-F. Li, and D. S. Seferos, "The rise of organic electrode materials for energy storage." *Chem. Soc. Rev.*, **45**, 6345 (2016).
20. K. Lin, Q. Chen, M. R. Gerhardt, L. Tong, S. B. Kim, L. Eisenach, A. W. Valle, D. Hardee, R. G. Gordon, and M. J. Aziz, "Alkaline quinone flow battery." *Science*, **349**, 1529 (2015).
21. T. Janoschka, N. Martin, U. Martin, C. Friebe, S. Morgenstern, H. Hiller, M. D. Hager, and U. S. Schubert, "An aqueous, polymer-based redox-flow battery using non-corrosive, safe, and low-cost materials." *Nature*, **527**, 78 (2015).
22. K. Lin, R. Gómez-Bombarelli, E. S. Beh, L. Tong, Q. Chen, A. Valle, A. Aspuru-Guzik, M. J. Aziz, and R. G. Gordon, "A redox-flow battery with an alloxazine-based organic electrolyte." *Nat. Energy*, **1**, 1 (2016).
23. B. Yang, L. Hoober-Burkhardt, S. Krishnamoorthy, A. Murali, G. S. Prakash, and S. Narayanan, "High-performance aqueous organic flow battery with quinone-based redox couples at both electrodes." *J. Electrochem. Soc.*, **163**, A1442 (2016).
24. B. Yang, L. Hoober-Burkhardt, F. Wang, G. S. Prakash, and S. Narayanan, "An inexpensive aqueous flow battery for large-scale electrical energy storage based on water-soluble organic redox couples." *J. Electrochem. Soc.*, **161**, A1371 (2014).
25. Y. Ding, C. Zhang, L. Zhang, Y. Zhou, and G. Yu, "Molecular engineering of organic electroactive materials for redox flow batteries." *Chem. Soc. Rev.*, **47**, 69 (2018).
26. B. Yang, L. Hoober-Burkhardt, S. Krishnamoorthy, A. Murali, G. S. Prakash, and S. Narayanan, "High-performance aqueous organic flow battery with quinone-based redox couples at both electrodes." *J. Electrochem. Soc.*, **163**, A1442 (2016).
27. P. Monk, *Viologens* (Wiley, New York, NY) (1998).
28. C. Bird and A. Kuhn, "Electrochemistry of the viologens." *Chem. Soc. Rev.*, **10**, 49 (1981).
29. R. J. Mortimer, D. R. Rosseinsky, and P. M. Monk, *Electrochromic Materials and Devices* (Wiley, New York, NY) (2015).
30. L. Liu, Y. Yao, Z. Wang, and Y.-C. Lu, "Viologen radical stabilization by molecular spectators for aqueous organic redox flow batteries." *Nano Energy*, **84**, 105897 (2021).
31. B. Hu, C. DeBruler, Z. Rhodes, and T. L. Liu, "Long-cycling aqueous organic redox flow battery (AORFB) toward sustainable and safe energy storage." *JACS*, **139**, 1207 (2017).
32. B. Hu, Y. Tang, J. Luo, G. Grove, Y. Guo, and T. L. Liu, "Improved radical stability of viologen anolytes in aqueous organic redox flow batteries." *Chem. Commun.*, **54**, 6871 (2018).
33. B. Hu and T. L. Liu, "Two electron utilization of methyl viologen anolyte in nonaqueous organic redox flow battery." *Journal of Energy Chemistry*, **27**, 1326 (2018).
34. C. DeBruler, B. Hu, J. Moss, X. Liu, J. Luo, Y. Sun, and T. L. Liu, "Designer two-electron storage viologen anolyte materials for neutral aqueous organic redox flow batteries." *Chem*, **3**, 961 (2017).
35. Y. Zhang, M. Li, S.-L. Li, and X.-M. Zhang, "The photochromic behaviour of two viologen salts modulated by the distances between the halide anions and the cationic N atoms of viologen." *Acta Crystallographica section C: Structural Chemistry*, **75** (2019).
36. X.-Q. Yu, C. Sun, B.-W. Liu, M.-S. Wang, and G.-C. Guo, "Directed self-assembly of viologen-based 2D semiconductors with intrinsic UV–SWIR photoresponse after photo/thermo activation." *Nat. Commun.*, **11**, 1 (2020).
37. A. J. Bard, L. R. Faulkner, J. Leddy, and C. G. Zoski, *Electrochemical Methods: Fundamentals And Applications* (Wiley, New York, NY) (1980).
38. H. Van Dam and J. Ponjee, "Electrochemically generated colored films of insoluble viologen radical compounds." *J. Electrochem. Soc.*, **121**, 1555 (1974).
39. E. Nightingale Jr, "Phenomenological theory of ion solvation. Effective radii of hydrated ions, The." *J. Phys. Chem.*, **63**, 1381 (1959).
40. J. Speight, *Lange's Handbook of Chemistry* (McGraw-Hill Publishing, New York, NY) 12 (2005).
41. A. F. Barton, "Solubility parameters." *Chem. Rev.*, **75**, 731 (1975).
42. X. Wei, L. Cosimbescu, W. Xu, J. Z. Hu, M. Vijayakumar, J. Feng, M. Y. Hu, X. Deng, J. Xiao, and J. Liu, "Towards high-performance nonaqueous redox flow electrolyte via ionic modification of active species." *Adv. Energy Mater.*, **5**, 1400678 (2015).
43. J. D. Milshtein, A. P. Kaur, M. D. Casselman, J. A. Kowalski, S. Modekrutti, P. L. Zhang, N. H. Attanayake, cf Elliott, S. R. Parkin, and C. Risko, "High current density, long duration cycling of soluble organic active species for non-aqueous redox flow batteries." *Energy Environ. Sci.*, **9**, 3531 (2016).
44. E. S. Beh, D. De Porcellinis, R. L. Gracia, K. T. Xia, R. G. Gordon, and M. J. Aziz, "A neutral pH aqueous organic–organometallic redox flow battery with extremely high capacity retention." *ACS Energy Lett.*, **2**, 639 (2017).
45. J. Luo, B. Hu, C. Debruler, Y. Bi, Y. Zhao, B. Yuan, M. Hu, W. Wu, and T. L. Liu, "Unprecedented capacity and stability of ammonium ferrocyanide catholyte in pH neutral aqueous redox flow batteries." *Joule*, **3**, 149 (2019).
46. A. A. Shinkle, A. E. Sleightholme, L. T. Thompson, and C. W. Monroe, "Electrode kinetics in non-aqueous vanadium acetylacetonate redox flow batteries." *J. Appl. Electrochem.*, **41**, 1191 (2011).
47. Y. Huang, S. Gu, Y. Yan, and S. F. Y. Li, "Nonaqueous redox-flow batteries: features, challenges, and prospects." *Current Opinion in Chemical Engineering*, **8**, 105 (2015).
48. X. Wei, W. Duan, J. Huang, L. Zhang, B. Li, D. Reed, W. Xu, V. Sprenkle, and W. Wang, "A high-current, stable nonaqueous organic redox flow battery." *ACS Energy Lett.*, **1**, 705 (2016).
49. X. Wang, X. Xing, Y. Huo, Y. Zhao, Y. Li, and H. Chen, "Study of tetraethylammonium bis (trifluoromethylsulfonyl) imide as a supporting electrolyte for an all-organic redox flow battery using benzophenone and 1, 4-di-tert-butyl-2,5-dimethoxybenzene as active species." *Int. J. Electrochem. Sci.*, **13**, 6676 (2018).
50. A. Nakahara and J. H. Wang, "Charge-transfer complexes of methylviologen." *J. Phys. Chem.*, **67**, 496 (1963).
51. P. M. Monk and N. M. Hodgkinson, "Charge-transfer complexes of the viologens: effects of complexation and the rate of electron transfer to methyl viologen." *Electrochim. Acta*, **43**, 245 (1998).
52. P. M. Monk, N. M. Hodgkinson, and R. D. Partridge, "The colours of charge-transfer complexes of methyl viologen: effects of donor, ionic strength and solvent." *Dyes Pigm.*, **43**, 241 (1999).

53. T. Mubita, J. Dykstra, P. Biesheuvel, A. Van Der Wal, and S. Porada, "Selective adsorption of nitrate over chloride in microporous carbons." *Water Res.*, **164**, 114885 (2019).
54. R. Nazmutdinov, P. Quaino, E. Colombo, E. Santos, and W. Schmickler, "A model for the effect of ion pairing on an outer sphere electron transfer." *Phys. Chem. Chem. Phys.*, **22**, 13923 (2020).
55. N. Hung and Z. Nagy, "Kinetics of the ferrous/ferric electrode reaction in the absence of chloride catalysis." *J. Electrochem. Soc.*, **134**, 2215 (1987).
56. X. Wei, W. Xu, M. Vijayakumar, L. Cosimbescu, T. Liu, V. Sprenkle, and W. Wang, "TEMPO-based catholyte for high-energy density nonaqueous redox flow batteries." *Adv. Mater.*, **26**, 7649 (2014).
57. A. Orita, M. Verde, M. Sakai, and Y. Meng, "The impact of pH on side reactions for aqueous redox flow batteries based on nitroxyl radical compounds." *J. Power Sources*, **321**, 126 (2016).
58. D. L. Marshall, M. L. Christian, G. Gryn'ova, M. L. Coote, P. J. Barker, and S. J. Blanksby, "Oxidation of 4-substituted TEMPO derivatives reveals modifications at the 1-and 4-positions." *Org. Biomol. Chem.*, **9**, 4936 (2011).